PROTEINS: Structure, Function, and Bioinformatics 53:130–141 (2003)

Conformational Interconversion in Compstatin Probed With Molecular Dynamics Simulations

Buddhadeb Mallik,[1] John D. Lambris,[2] and Dimitrios Morikis[1]*
[1]*Department of Chemical and Environmental Engineering, University of California at Riverside, Riverside, California*
[2]*Department of Pathology and Laboratory Medicine, University of Pennsylvania, Philadelphia, Pennsylvania*

ABSTRACT **Compstatin is a 13-residue cyclic peptide that has the potential to become a therapeutic agent against unregulated complement activation. In our effort to understand the structural and dynamic characteristics of compstatin that form the basis for rational and combinatorial optimization of structure and activity, we performed 1-ns molecular dynamics (MD) simulations. We used as input in the MD simulations the ensemble of 21 lowest energy NMR structures, the average minimized structure, and a global optimization structure. At the end of the MD simulations we identified five conformations, with populations ranging between 9% and 44%. These conformations are as follows: 1) coil with α_R-α_R β-turn, as was the conformation of the initial ensemble of NMR structures; 2) β-hairpin with ϵ-α_R β-turn; 3) β-hairpin with α_R-α_R β-turn; 4) β-hairpin with α_R-β β-turn; and 5) α-helical. Conformational switch was possible with small amplitude backbone motions of the order of 0.1–0.4 Å and free energy barrier crossing of 2–11 kcal/mol. All of the 21 MD structures corresponding to the NMR ensemble possessed a β-turn, with 14 structures retaining the α_R-α_R β-turn type, but the average minimized structure and the global optimization structures were converted to α-helical conformations. Overall, the MD simulations have aided to gain insight into the conformational space sampled by compstatin and have provided a measure of conformational interconversion. The calculated conformers will be useful as structural and possibly dynamic templates for optimization in the design of compstatin using structure-activity relations (SAR) or dynamics-activity relations (DAR). Proteins 2003;53:130–141.**

Key words: compstatin; complement; inhibitor; peptide; NMR; secondary structure; structure; beta-turn; molecular dynamics

INTRODUCTION

Compstatin is a complement inhibitor peptide that binds specifically to human and primate complement component C3 and inhibits the cleavage of C3 to C3a and C3b, thus disrupting the cascade of complement activation.[1,3] Unregulated complement activation is involved in a number of autoimmune diseases, trauma, transplantation, myocardial and cerebral ischemia reperfusion injury, and in bioincompatibility situations with biomaterial during cardiopulmonary bypass surgery.[4,5] Compstatin has been tested and shown to be effective in a number of studies using in vitro, in vivo, ex vivo, and in vivo/ex vivo interface models[1,3,6–9] with low toxicity.[3,6] This C3 inhibitor was first identified as a 27-residue peptide, by screening a phage-displayed random peptide library against C3.[1] It was shown that the 13-residue cyclic N-terminal segment of the peptide was sufficient and the shortest segment for inhibitory activity.[1,2] This peptide, named compstatin, has the sequence Ile1-[Cys2-Val3-Val4-Gln5-Asp6-Trp7-Gly8-His9-His10-Arg11-Cys12]-Thr13-NH_2, where the residues in brackets denote a cyclic ring formed by a disulfide bridge between Cys2 and Cys12.[1,10] Further studies showed that addition of an acetyl blocking group at the N-terminus resulted to approximately a threefold increase in inhibitory activity.[2,3]

The three-dimensional structure of compstatin in solution was determined by using NMR spectroscopy and computational methodologies based on hybrid distance geometry-simulated annealing[10] and global optimization.[11] The molecular surface of compstatin consists of a predominantly polar part and a predominantly hydrophobic part. The polar part contains an α_R-α_R (type I) β-turn comprising residues Gln5-Asp6-Trp7-Gly8, and the hydrophobic part contains the disulfide bridge.[10,12] Structure-activity relations (SAR) using an Ala scan and residue substitutions, which introduced perturbations in the structural stability of compstatin, showed the following: 1) the four residues of the β-turn, the disulfide bridge, and Val3 of the hydrophobic surface are essential for inhibitory

Abbreviations: MD, molecular dynamics; ES1-21, ensemble of NMR structures; AMS, averaged minimized structure; GOS, global optimization structure; MD1-21, MD structures corresponding to initial ES1-21 structures; MDAMS, MD structure corresponding to AMS initial structure; MDGOS, MD structure corresponding to GOS initial structure; GB, generalized Born; ABNR, adopted-basis Newton-Raphson; C3, complement component C3; Ac, acetyl; SAR, structure-activity relations; DAR, dynamics-activity relations; RMSD, root-mean-square deviation.

Grant sponsor: American Heart Association, Western States Affiliate; Grant number: 0255757Y; Grant sponsor: National Institutes of Health; Grant number: GM 62134.

Correspondence to: Dimitrios Morikis, Department of Chemical and Environmental Engineering, University of California at Riverside, Riverside, CA 92521. E-mail: dmorikis@engr.ucr.edu

Received 24 February 2003; Accepted 14 April 2003

activity; 2) the β-turn is a necessary but not a sufficient condition for activity; 3) the linear sequence of compstatin has propensity for turn formation; 4) Val3 is necessary for activity and its substitution to Ala results in stronger (higher population) turn; (5) the β-turn residues Gln5(Asn5)-Asp6-Trp7(Phe7)-Gly8 are specific for turn formation but only Gln5(Asn5)-Asp6-Trp7-Gly8 are specific for activity; this finding suggests that Trp7 may be directly participating to binding.[10,12]

The above studies revealed a sequence template with highest activity as Ac-Xaa-[Cys2-Val3-Xaa-Gln5-Asp6-Trp7-Gly8-Xaa-Xaa-Xaa-Cys12]-Xaa-NH_2, where Xaa denotes residues that can be amenable to further optimization. Additional studies aimed to optimize the activity of compstatin by optimizing its sequence at positions Xaa, using the following: 1) rational design, 2) experimental combinatorial design of a phage-displayed random peptide library, and 3) computational combinatorial design. Rational design yielded an acetylated analog with a His9Ala substitution, called Ac-H9A, which was 1.6-fold more active than acetylated compstatin, Ac-compstatin.[12] In the phage-displayed random peptide library, only residues Xaa were allowed to combinatorially vary. Screening of this library against C3 also yielded an analog with triple replacement Ile1Leu/His9Trp/Thr13Gly, called Ac-I1L/H9W/T13G, which was 1.6-fold more active than Ac-compstatin (Soulika AM, Morikis D, Sarrias M-R, Roy M, Spruce LA, Sahu A, Lambris JD. Studies of structure-activity relations of complement inhibitor compstatin. Journal of Immunology 2003: In Press). The computational combinatorial design, based on global optimization against the structural template of compstatin, yielded an analog with double replacement Val4Tyr/His9Ala, called Ac-V4Y/H9A, which was sevenfold more active than Ac-compstatin (Klepeis JL, Floudas CA, Morikis D, Tsokos CG, Argyropoulos E, Spruce L, Lambris JD. Integrated computational and experimental approach for lead optimization and design of compstatin variants with improved activity. Journal of the American Chemical Society 2003: In Press).

It is obvious that the activity optimization studies depend on the available structural template of compstatin. It is also well known that small peptides in solution form ensembles of interconverting conformers. The NMR structure of compstatin is consistent with the presence of a major conformer with the main characteristic of the formation of the α_R-α_R β-turn opposite to the disulfide bridge.[10] To identify conversion to additional conformers, we performed molecular dynamics (MD) simulations with starting structures each of the 21 from the ensemble of structures, the averaged minimized structure, and the global optimization structure of compstatin, using a continuum solvent model and a more complete energy function than the one typically used for NMR structure determination.

MATERIALS AND METHODS

We have performed MD simulations for a family of NMR-derived structures of compstatin. The family includes the ensemble of structures (ES) that consists of 21 lowest energy structures (PDB Code 1a1p[10]), the average minimized structure (AMS[10]), and the global optimization structure (GOS[11]). The output structures were named accordingly MD1-21, MDAMS, and MDGOS. The simulation was done with the CHARMM program version c28a4,[13] using the topology and parameter files toph19 and paramh19, respectively. A charged N-terminus was used with the normal patch NTER (NH_3^+). To account for the experimental C-terminal blocking group NH_2, the C-terminal residue Thr was changed to Thr–NH_2. The topology and parameters for the new amidated C-terminus were adopted from the CHARM22 all-hydrogen protein topology top_all22_prot.inp and parameters par_all22_prot.inp, respectively.

Our empirical energy function had the form $E = E_{int} + E_{nb} + E_{solv}$, where E_{int} refers to the internal energy terms (E_{bond}, E_{angle}, $E_{torsion}$, $E_{improper}$), E_{nb} includes all nonbonded interaction terms (E_{vdW}, E_{elec}, E_{hb}), and E_{solv} is the solvation energy. Standard CHARMM energy terms were used. E_{bond} and E_{angle} were modeled as harmonic potentials. The four-atom torsion energy term $E_{torsion}$ was defined by a periodic potential characterized by different energy constants and different periodicity for a given set of four atoms. A quadratic distortion potential was used for $E_{improper}$. For E_{vdW}, a 6–12 Lennard-Jones potential was used with a switching function. E_{elec} was modeled as pairwise Coulomb's potential with a similar kind of switching or shifting functions to account for the cutoffs used in nonbonded interactions. E_{hb} was again a vdW-type potential with more complex terms in it and exponents are different. Part of the solvation energy is correlated with solvent-accessible surface area of atoms. The electrostatic polarization energy contribution of the solvation energy is the sum of Coulomb's term in a dielectric medium and the Born term. These together constitute the generalized Born (GB) solvation energy term.[14] In our MD simulation, we included electrostatic effects through Coulomb's terms using a constant dielectric of 1. The solvent effect was incorporated in CHARMM[15] through the generalized Born (GB) implicit solvation model. No spherical truncation was applied for the nonbonded interactions. Typical NMR structure determinations using hybrid distance geometry-simulated annealing protocols do not include electrostatic, explicit hydrogen bond, and solvation energy terms, and the van der Waals is a repel energy term, as was the case for compstatin.[10] The integration time step was 2 fs with bonds to hydrogen atoms constrained to a fixed value by SHAKE.[16] All simulations were performed at 300 K. Before the initiation of the actual dynamics run, a 300-steps adopted-basis Newton-Raphson (ABNR) minimization was performed for all structures to relax the van der Waals contacts if any. A disulfide patch between CYS2 and CYS12 was used to keep the disulfide bond intact, which otherwise is very unstable and gets severed almost at the beginning of dynamics.

Initial 200-ps MD simulations with a timestep of 2 fs were performed to test the behavior of the system. Then, separate 1-ns MD simulations were performed by using the same setup as the 200-ps simulations. These entailed

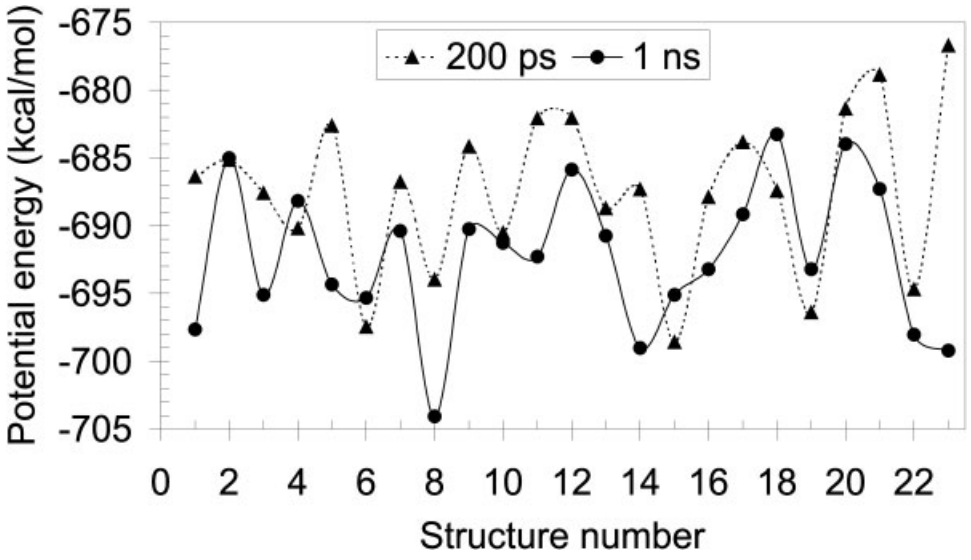

Fig. 1. Potential energy of each model of the family of compstatin structures used in the MD simulations. The energy values represent the average of the last 6 ps of the 200-ps MD simulation and the 1-ns MD simulation.

23 MD runs corresponding to the 23 initial structures mentioned above. After the initial minimization, the MD simulation was performed with a timestep of 2 fs up to 1 ns. Each MD trajectory was saved at every 2 ps. The MD average energy of the last 6-ps run of all the structures is plotted in Figure 1 for the initial 200-ps and final 1-ns simulations. All structures lie within a narrow range of energy (690 ± 15 kcal/mol), and small improvement is observed going from 200 ps to 1 ns. There is essentially no correlation between the potential energies after 200 ps and 1 ns (Fig. 1).

RESULTS

We have performed 1-ns MD simulations in combination with NMR three-dimensional structures to gain insight into the conformational space that can be sampled by compstatin and the possibility of conformational interconversion. We used 23 initial structures, corresponding to the ensemble of the 21 lowest energy NMR structures (ES1-21), the averaged minimized structure (AMS), and the global optimization structure (GOS). The respective MD structures were MD1-21, MDAMS, and MDGOS.

We have examined structural snapshots along the 23 MD trajectories to identify the conformational preference of each compstatin residue. Figure 2 shows the Ramachandran plots of the backbone (ϕ, ψ) dihedral angles for residues 2–12 of compstatin. The data points correspond to snapshots of structures from the complete 1-ns trajectories saved every 2 ps. Each panel contains 11,500 points corresponding to 500 snapshots × 23 structures of the ensemble. These panels depict the statistical occupancy of the (ϕ, ψ) space during the time of the simulation for each residue. The percent occupancy during the simulations is marked for four regions of the Ramachandran plot in Figure 2. We consider the Ramachandran plot divided in four regions using definitions from Wilmot and Thornton[17] with bounds as follows: 1) β-region, for ($\phi \leq 0°$, $\psi > 60°$, $\psi < -120°$); 2) α_R-region, for ($\phi \leq 0°$, $-120° \leq \psi \leq 60°$); 3) α_L/γ-region, for ($\phi > 0°$, $\psi < 110°$, $\psi > -70°$); 4) ε-region, for ($\phi > 0°$, $\psi \geq 110°$, $\psi \leq -70°$). This classification allows for variation in the dihedral angles in the β-, α_R-, and α_L/γ-regions and for generous variation in the ε-region. Figure 3 shows a graphic representation of these regions and corresponding β-turn types that are discussed below, and Table I summarizes the ideal β-turn types.

Residues Cys2, Val3, and Val4 show a statistical preference for the β-region and smaller preference for the α_R-region of the Ramachandran plot (Fig. 2). Residue Val3 shows a small population in the ε-region of the Ramachandran plot, which is typically populated by residue 2 of an ε-α_R β-turn (Fig. 2).

The following four residues, Gln5, Asp6, Trp7, and Gly8, correspond to the α_R-α_R β-turn of the parent structures. Residue Gln5 populates all four quadrants of the Ramachandran plot with population rank in the order of $\alpha_L > \beta > \alpha_R > \epsilon$, corresponding to a variety of structures (Fig. 2). The population rank of Asp6 is of the order of $\alpha_R > \epsilon > \beta > \alpha_L$ (Fig. 2). The population rank of Trp7 is of the order of $\alpha_R > \beta$ (Fig. 2). Gly8 populates regions characteristic of Gly residues.

The remaining four residues, His9, His10, Arg11, and Cys12, immediately after the β-turn of the parent structures, show statistical preference for the β-region of the Ramachandran plot, although with smaller populations than the three residues immediately before the β-turn, Cys2, Val3, and Val4 (Fig. 2). Specifically, His9 shows preference for the β-region of the Ramachandran plot, with population rank in the order of $\beta > \alpha_L > \alpha_R$. The population rank for His10 is $\alpha_R \approx \beta$, for Arg11 is $\beta \geq \alpha_R > \epsilon$, and for Cys12 is $\beta > \alpha_R$ (Fig. 2).

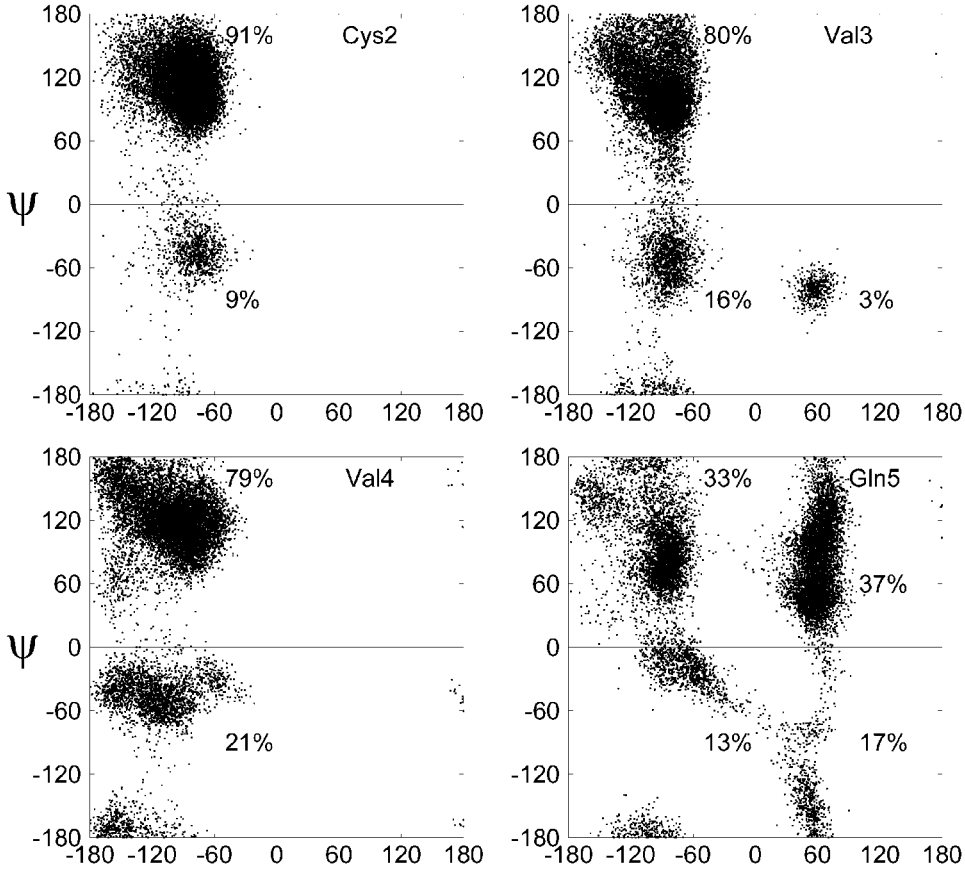

Fig. 2. Ramachandran plots showing the backbone (ϕ,ψ) conformational space of residues Cys2 to Cys12 of our family of compstatin structures during the 1-ns MD simulations. Individual panels correspond to each residue in the segment 2–12 and show the statistical (ϕ,ψ) distribution of 2-ps snapshot structures for all 23 models. Percent occupancies of each residue for the β-, α_R-, α_L/γ-, and ϵ-regions of the Ramachandran plot (defined in text) are labeled in each panel.

During the MD simulation we observed interconversion of a number of conformations. We examined in detail 10 structures at 100-ps intervals up to 1 ns, for each of the 23 initial structures (a total of 230 structures). Although the 100-ps interval is arbitrary, it is sufficient to provide a representative view of the conformational interconversion during the simulations. The observed secondary structures can be classified in 10 conformational clusters: 1) 95 structures in coil/α_R-α_R (41.3% population), 2) 50 in β-hairpin/α_R-α_R (21.7%), 3) 26 in β-hairpin/ϵ-α_R (11.3%), 4) 20 in coil/ϵ-α_R (8.7%), 5) 14 in α-helix (6.1%), 6) 11 in coil/α_R-β (4.8%), 7) 6 in coil/β-α_R (2.6%), 8) 5 in 3_{10}-helix (2.2%), 9) 2 in β-hairpin/γ-α_R (0.9%), and 10) 1 in β-hairpin/3_{10}-helix (0.4%). Table II summarizes the observed conformations after the initial minimization and during the MD simulation for each of the 23 initial structures. For simplicity of presentation, we have included in Table II the conformations every 200 ps, although our analysis, above, was performed every 100 ps.

The final structures at the end of the MD simulation clustered into five families of secondary structure presented in Figure 4. The final families of structures are as follows: 1) 10 structures in coiled conformations with the presence of an α_R-α_R β-turn [Fig. 4(A)], as was the case of the 23 initial structures used in the MD simulation (note that the α_R-α_R region includes type I and type III β-turns; Fig. 2; Table I); 2) 4 structures in β-hairpin conformation with the presence of an α_R-α_R β-turn [Fig. 4(B)]; 3) 5 structures in β-hairpin conformations with the presence of an ϵ-α_R β-turn [Fig. 4(C)]; 4) 2 structures in β-hairpin conformation with the presence of an α_R-β β-turn [Fig. 4(D)]; and 6) 2 structures in α-helical conformation [Fig. 4(E)].

Secondary structure classification to coil, β-sheet, or α-helix was made by using the algorithm by Kabsch and Sander[18] implemented within the program MOLMOL.[19] Further classification of β-turns was made according to the criteria of Wilmot and Thornton,[17,20] summarized in Table I. Here we follow the Ramachandran nomenclature and classification established by Thornton and coworkers,[17,20–22] which represents the β-turn types according to the conformational space of the backbone dihedral angles (ϕ,ψ) of residues 2 and 3 of the turns (Table I and Fig. 3). This classification is more general and accounts for the inclusion into the same category of β-turns of types I and III, the distinction of which has been the subject of concern

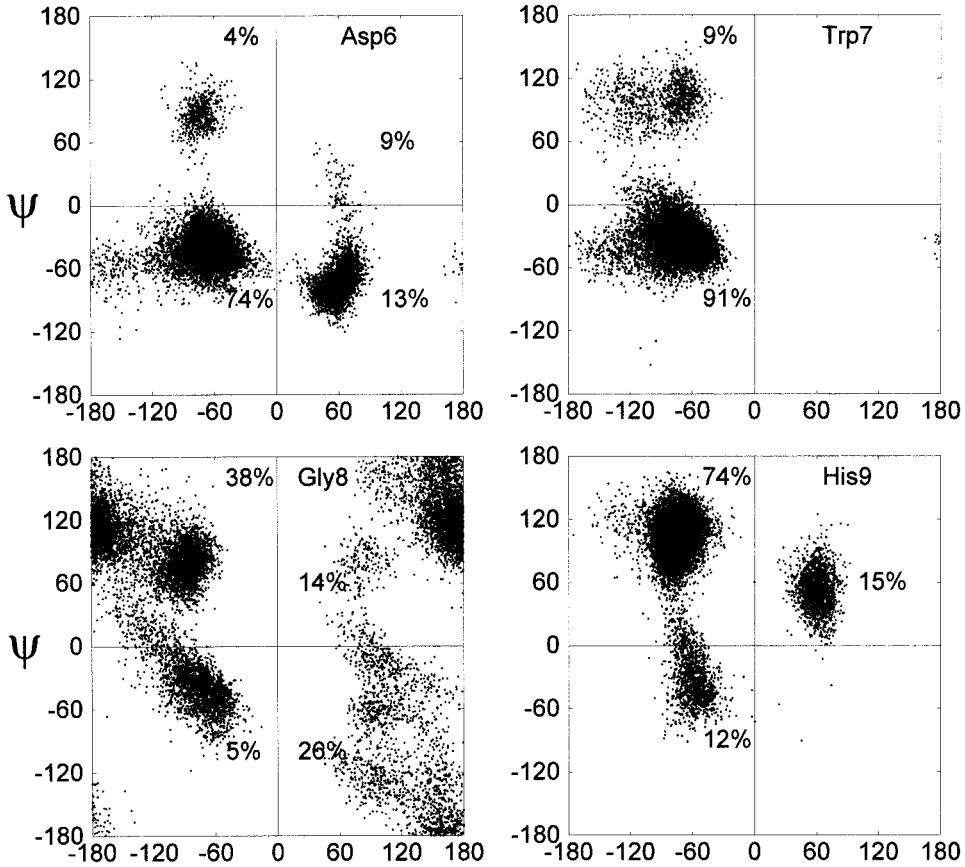

Figure 2 (Continued.)

in the past.[17,20,23–27] An excellent recent review on tight turns in general, including two- to six-residue turns, can be found in Ref. 28.

Specifically, the 10 initial structures ES1,2,3,5,7,8, 12,14,19,20 converged to coiled conformations with α_R-α_R β-turns, spanning the segment 5–8 at the end of the MD simulation (Table II). We call this family of structures collectively coil/α_R-α_R (Table III).

Initial structures ES4,13,17,18 converged to β-hairpin conformations with α_R-α_R β-turns spanning the segment 5–8 (Table II). We call this family of structures collectively β-hairpin/α_R-α_R (Table III). Initial structures ES9,10,11,16,21 also converged to β-hairpin conformations, but with ϵ-α_R β-turns, spanning the segment 5-8 (Table II). We call this family of structures collectively β-hairpin/ϵ-α_R (Table III). Initial structures ES6,15 converged to a β-hairpin conformation with α_R-β β-turn, spanning the segment 5–8 (Table II). We call this single structure family β-hairpin/α_R-β (Table III). Alternatively, these structures could be classified as possessing a β-γ β-turn in the segment 6–9 (shifted by one residue). However, we rejected this classification because it leaves Asp6 in the ϵ-region, which is disallowed except for a second residue of an ϵ-α_R β-turn.

Finally, initial structures AMS and GOS converged to α-helical conformations, spanning the segments 5–9 (MDAMS) and 8–12 (MDGOS), respectively (Tables II and III). This is not unusual because the turns of α-helices or 3_{10}-helices are located in the α_R-α_R region in the Ramachandran plot (Table I). It is not clear to us if the rapid conversion to α-helix for the averaged minimized and global optimization structures is fortuitous (Table II). The use of averaged minimized NMR structures is typical in most theoretical studies appearing in literature. This is because it is assumed that averaged minimized NMR structures are good representations of NMR conformational ensembles. However, our MD studies of compstatin indicate that the use of the complete NMR ensemble of structures provides a more complete representation of the conformational space, which has a strong and diverse impact on the theoretical results.

Figure 5 shows the three β-turn types that are present in the nonhelical MD structures (Table III) to provide a visual assessment of the turn qualities. The region shown is for residues Gln5-Asp6-Trp7-Gly8. Fourteen structures contain an α_R-α_R β-turn [Fig. 5(A)], 5 structures contain an ϵ-α_R β-turn [Fig. 5(B)], and 2 structures contain an α_R-β β-turn [Fig. 5(C)].

Figure 6 shows plots of the mean RMSD between the final MD and the initial NMR structures for the backbone heavy atoms. The plots correspond to the five families of MD structures. Examination of the middle residues of the β-turn, Asp6 and Trp7, indicates that average backbone motions of

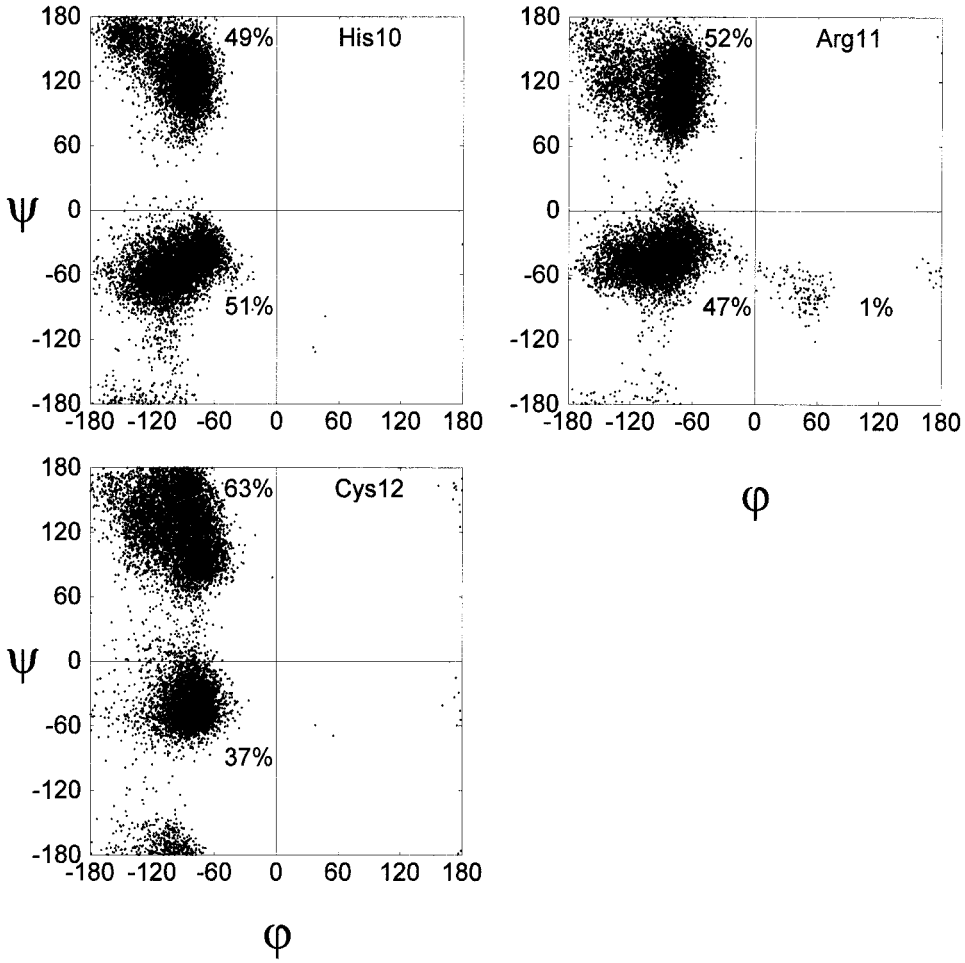

Figure 2. (Continued.)

TABLE I. Dihedral Angles of Ideal β-Turns[a]

Turn type		Dihedral angles[a,b]			
		φ_2	ψ_2	φ_3	ψ_3
α_R-α_R[c]	I	−60	−30	−90	0
	III	−60	−30	−60	−30
α_L-γ	I′	60	30	90	0
α_L-α_L	III′	60	30	60	30
β-γ	II	−60	120	80	0
ε-α_R	II′	60	−120	−80	0
α_R-β	VIII	−60	−30	−120	120

[a]Dihedral angle values are from Lewis et al.[24] and are allowed to vary by ±30°, with one angle allowed to deviate by as much as ±45°. Additional criteria for β-turn formation are as follows: the distance between α-carbon atoms 1 and 4 of β-turn C_1^{α}-$C_4^{\alpha} < 7.0$ Å, and the central turn residues are not helical.

[b]Subscripts 2 and 3 refer to residues 2 and 3 of the β-turn.

[c]Nomenclature introduced by Thornton and coworkers using allowed regions of the Ramachandran plot, where the first component denotes the conformational space of residue 2 and the second component denotes the conformational space of residue 3 of the β-turn.[17,20–22]

0.2–0.4 Å can result in β-turn switch. For example, a ~0.2 Å motion for the backbone of Asp6 results to switch between α_R-α_R to ε-α_R β-turn; and a ~0.4 Å motion for the backbone of Trp7 results to switch between α_R-α_R and α_R-β. Average backbone motions of as little as 0.1 Å are sufficient for coil-hairpin switch. This gives us an indication of the amplitudes of the motions that are involved in the backbone conformational interconversion of compstatin.

We have calculated the average total energies of each MD family of structures at 1 ns. Figure 7 shows a plot of the free energy minima for the five families of MD structures. Because these total energies include solvation terms implicitly, the difference between two energy minima can be approximated as the free energy barrier, assuming that the entropy terms do not vary significantly. Figure 7 shows that the energy barriers lie within 2–11 kcal/mol. In essence, this plot indicates that free energy barrier for coil-hairpin conversion is of the order of 2–5 kcal/mol, for coil-helix conversion is of the order of 6 kcal/mol, and for hairpin-helix conversion is of the order of 3–11 kcal/mol. Compensatory effects for loss or gain of side-chain or turn backbone hydrogen bonds may also be present.

DISCUSSION

The structure of a major conformer of compstatin was previously determined by using NMR-derived restraints

TABLE II. Conformational Interconversion During the 1-ns MD Simulation

Model[a]	Minimization t = 0 ps	t = 200 ps	t = 400 ps	t = 600 ps	t = 800 ps	t = 1000 ps
ES1	Coil/α_R-α_R	Coil/α_R-α_R	Coil/α_R-α_R	Coil/α_R-α_R	Coil/α_R-α_R	Coil/α_R-α_R
ES2	Coil/α_R-α_R	Coil/α_R-α_R	Coil/α_R-α_R	Coil/α_R-α_R	Coil/α_R-α_R	Coil/α_R-α_R
ES3	Coil/α_R-α_R	Coil/α_R-α_R	Coil/α_R-α_R	Coil/α_R-α_R	Coil/α_R-α_R	Coil/α_R-α_R
ES4	Coil/α_R-α_R	β-hairpin/α_R-α_R	β-hairpin/α_R-α_R	β-hairpin/α_R-α_R	Coil/α_R-α_R	β-hairpin/α_R-α_R
ES5	Coil/α_R-α_R	β-hairpin/α_R-α_R	β-hairpin/α_R-α_R	β-hairpin/α_R-α_R	β-hairpin/α_R-α_R	Coil/α_R-α_R
ES6	Coil/α_R-α_R	3_{10}-helix	β-hairpin/α_R-α_R	3_{10}-helix	β-hairpin/α_R-α_R	β-hairpin/α_R-α_R
ES7	Coil/α_R-α_R	Coil/α_R-α_R	Coil/α_R-α_R	Coil/α_R-α_R	Coil/α_R-α_R	Coil/α_R-α_R
ES8	Coil/α_R-α_R	Coil/ε-α_R	Coil/ε-α_R	Coil/ε-α_R	Coil/ε-α_R	Coil/α_R-α_R
ES9	Coil/α_R-α_R	Coil/α_R-α_R	Coil/α_R-α_R	Coil/α_R-α_R	Coil/ε-α_R	β-hairpin/ε-α_R
ES10	Coil/α_R-α_R	Coil/α_R-α_R	β-hairpin/ε-α_R	β-hairpin/ε-α_R	β-hairpin/ε-α_R	β-hairpin/ε-α_R
ES11	3_{10}-helix	β-hairpin/ε-α_R	β-hairpin/ε-α_R	Coil/ε-α_R	β-hairpin/ε-α_R	β-hairpin/ε-α_R
ES12	Coil/α_R-α_R	β-hairpin/α_R-α_R	β-hairpin/α_R-α_R	β-hairpin/α_R-α_R	β-hairpin/α_R-α_R	Coil/α_R-α_R
ES13	Coil/α_R-α_R	β-hairpin/α_R-α_R	β-hairpin/α_R-α_R	Coil/α_R-α_R	Coil/α_R-α_R	β-hairpin/α_R-α_R
ES14	Coil/α_R-α_R	Coil/α_R-α_R	Coil/α_R-α_R	Coil/α_R-α_R	Coil/α_R-α_R	Coil/α_R-α_R
ES15	Coil/α_R-α_R	Coil/α_R-β	Coil/α_R-β	Coil/α_R-β	Coil/α_R-β	Coil/α_R-β
ES16	Coil/α_R-α_R	Coil/ε-α_R	Coil/ε-α_R	Coil/ε-α_R	Coil/ε-α_R	β-hairpin/ε-α_R
ES17	Coil/α_R-α_R	β-hairpin/α_R-α_R	β-hairpin/α_R-α_R	Coil/α_R-α_R	β-hairpin/α_R-α_R	β-hairpin/α_R-α_R
ES18	3_{10}-helix	Coil/α_R-α_R	Coil/α_R-α_R	β-hairpin/α_R-α_R	β-hairpin/α_R-α_R	β-hairpin/α_R-α_R
ES19	Coil/α_R-α_R	Coil/α_R-α_R	Coil/α_R-α_R	Coil/α_R-α_R	Coil/α_R-α_R	Coil/α_R-α_R
ES20	3_{10}-helix	Coil/ε-α_R	Coil/α_R-α_R	Coil/α_R-β	β-hairpin/α_R-α_R	Coil/α_R-α_R
ES21	Coil/α_R-α_R	Coil/ε-α_R	β-hairpin/ε-α_R	β-hairpin/3_{10}-helix	β-hairpin/ε-α_R	β-hairpin/ε-α_R
AMS	Coil/α_R-α_R	α-helix	α-helix	α-helix	α-helix	α-helix
GOS	Coil/α_R-α_R	α-helix	α-helix	Coil/β-α_R	Coil/β-α_R	α-helix

[a]ES1-21 are the initial NMR structures, AMS is the averaged minimized structure, and GOS is the global optimization structure.

and a hybrid distance geometry-simulating annealing protocol.[10] The major conformer of compstatin possessed an α_R-α_R β-turn, spanning residues Gln5-Asp6-Trp7-Gly8. It was estimated by using $^3J_{HN\text{-}H\alpha}$-coupling constant analysis, that the major conformer of compstatin had a population of 42–63%.[10] It was also shown with use of chemical shift analysis that compstatin was in a flexible conformational environment.[10] Finally, two side-chains, Trp7 and Gln5, were observed in alternative low-population conformations, with an estimate of 4% for the low populations of Trp7.[10] The structure of compstatin was also determined by using a novel global optimization methodology and a subset of the NMR restraints.[11] The hybrid distance geometry-simulating annealing structure and the global optimization structure were in excellent agreement for the β-turn region (residues 5–8) and in fair agreement for the best defined region (residues 3–9). The best-defined region comprises the residues that show long-range Nuclear Overhauser Effect (NOE)s involving side-chains.

Small peptides are very flexible in solution and assume multiple interconverting conformations.[29,30] Then, NMR observables, such as chemical shifts, cross-peak volumes and line widths, coupling constants, and NOEs, are averaged over several conformations. In certain instances, one conformer may be sufficiently populated to dominate the measurable NMR observables and a complete three-dimensional structure determination is possible. This is the case for both linear and cyclic peptides, although cyclic peptides are conformationally more restrained than linear peptides and more likely to be amenable to structure determination by NMR. Several NMR studies have shown the presence of alternative conformations in peptides,

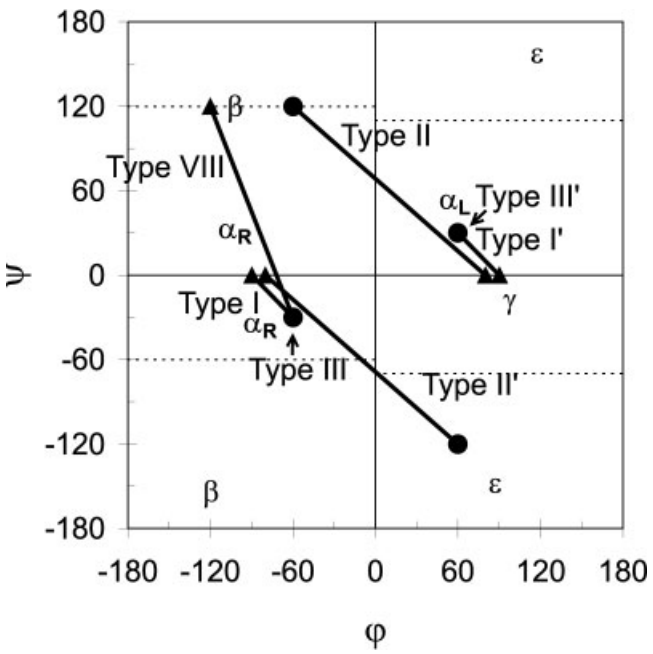

Fig. 3. Conformational space of ideal β-turns in Ramachandran plot[17,20–27] using the traditional nomenclature (marked in figure) and the one defined by Thornton and coworkers[17,20–22] used here (see also Table I for nomenclature correspondance). Solid circles correspond to (ϕ_2,ψ_2) and solid triangles correspond to (ϕ_3,ψ_3), where subscripts denote residues 2 and 3 of the β-turn. The (ϕ,ψ) space has been divided into four regions separated by dotted lines, β, α_R, α_L/γ, and ϵ (marked in figure), as defined in text.

including isolated β-turns,[31,32] nascent helices,[33] α-helices,[34–36] mixtures of 3_{10}-α-helices,[37] β-hairpins,[38–40] three-stranded β-sheets,[41,42] and covalently linked peptides

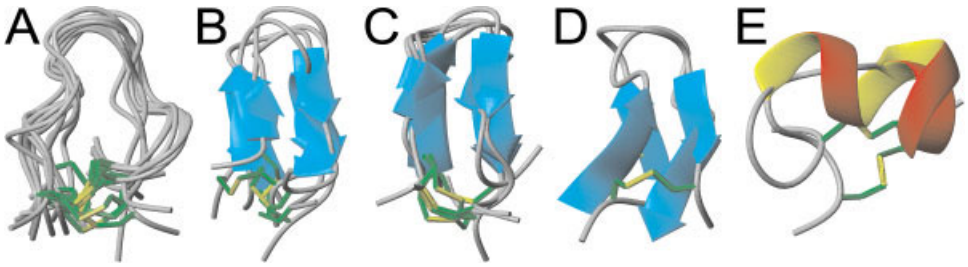

Fig. 4. The five families of compstatin structures derived by MD simulations. **A:** Coil with α_R-α_R β-turn. **B:** β-Hairpin with α_R-α_R β-turn. **C:** β-Hairpin with ε-α_R β-turn. **D:** β-Hairpin with α_R-β β-turn. **E:** α-Helix. The disulfide bridge is drawn in yellow and the C^{α}-C^{β}-S^{γ} bonds are drawn in green. The β-turn is located opposite to the disulfide bridge in (A–D). The classification for each individual structure is given in Table II and collectively for each family is given in Table III.

with β-sheets and double β-turns.[43] This has also been the case in compstatin, which is a conformtionally restrained 13-residue peptide with an 11-residue ring, cyclized with a disulfide bridge between residues Cys2 and Cys12. The original structure determination studies,[10] as their authors pointed out, showed evidence of multiple conformations with an observable population of an α_R-α_R β-turn.

To further investigate the conformational freedom of compstatin and to detect possible alternative low-population conformations, we have performed MD simulations of the ensemble of 21 low-energy structures, the average minimized structure, and the global optimization structure. These calculations include implicit interactions with continuum solvent representation and a complete target energy function with covalent geometry, 6–12 Lennard-Jones van der Waals interactions, Coulombic interactions, and hydrogen-bonding interactions, but they do not include experimental NMR restraints. Our choice to use 23 initial structures in our MD simulations, as opposed to a single crystallographic or average minimized NMR structure, are rationalized below.

It should be noted that NMR structures are typically presented as ensembles of low-energy structures that converge to the same (high population) conformer with low RMSD and without violating certain experimental criteria for NMR-derived or deduced restraints. The RMSD is a measure of the precision of the structures and an indication of the variation of the local conformational space that is allowed without violating the experimental restraint criteria. Typically, NMR ensembles show low RMSD for regular well-formed secondary structure such as α-helices and β-pleated sheets, higher RMSD for turns, and even higher RMSD for loops. In this sense, the RMSD can also be a measure of the flexibility of the local secondary structure. Sometimes high RMSD is caused by deficits in NMR observables such as NOEs (distance restraints), J-coupling restraints, or torsion angle restraints. Such deficits may even be attributed to conformation flexibility, as evidenced in the averaged NMR observables, in cases where no other ambiguitites in the NMR assignments are caused by low spectral resolution and/or sensitivity, chemical shift degeneracy, or cross-peak overlap.

It was not clear to us, in small peptides such as compstatin, with a minimal single element secondary structure (a β-turn) and an unstructured region, what part of the structure will dominate the MD simulations and will persist to the end point of the dynamics. In addition, is it possible that the conformation of the unstructured or flexible high RMSD region of individual ensemble structures will be responsible for introducing alternative conformations, depending on the initial individual structure of the NMR ensemble?

Indeed, this was the case in compstatin. Our results show the presence of five families of structures at 1 ns (Table III), which provide a measure of the populations of interconverting conformers in compstatin. The family of structures with the largest population (43.5%) conforms to a coil conformation with the presence of an α_R-α_R β-turn (Table III). This conformation is consistent with the major conformer of compstatin derived by the NMR data.[10] The second largest population (21.7%) conforms to β-hairpin conformation with the presence of an ε-α_R β-turn (Table III). This population is more structured than the highest population because, besides the β-turn, the two sides of compstatin are in close proximity, which allows the formation of interstrand hydrogen bonds. The third population (17.4%) also conforms to a β-hairpin, and with a turn in the α_R-α_R region, as in the highest population (Table III). The fourth population (8.7%) also conforms to a β-hairpin, but with a turn in the α_R-β region (Table III). Coil-hairpin interconversion in compstatin is not surprising given the cyclic nature of the peptide and the presence of well-defined β-turn. The fifth population (8.7%) is composed of two structures with radically different conformation of α-helix (Table III). These are structures MDAMS and MDGOS that have resulted from the initial average minimized and global optimization structures, respectively. This is not surprising because α_R-α_R β-turns can also be half turns of 3_{10}- or α-helices. The α-helix has different starting and ending points and length in the two structures (Table II).

It is possible that the NMR-derived structural ensemble is undersampled compared to the calculated MD structural ensembles. This may be owed to differences in the target energy functions used in the NMR structure determination protocol and the MD simulation. In particular, we point out the absence of electrostatic interaction and solvation energy terms in the NMR protocol. However, it

TABLE III. Classification of β-Turns in Segment 5–8 of the MD Structures

Family	No. of models (population)	β-turn dihedral angles[a] Asp6 φ_2	Asp6 ψ_2	Trp7 φ_3	Trp7 ψ_3	C_α(Gln5)-C_α(Gly8) distance[b]
Coil/α_R-α_R	10 (43.5%)	−69.7 ± 11.6	−37.9 ± 20.7	−68.7 ± 22.0	−24.6 ± 23.2	5.5 ± 0.5
β-hairpin/α_R-α_R	4 (17.4%)	−71.1 ± 24.8	−33.7 ± 15.2	−88.7 ± 18.2	−37.2 ± 9.8	5.5 ± 0.7
β-hairpin/ε-α_R	5 (21.7%)	62.5 ± 7.4	−76.9 ± 19.8	−59.5 ± 6.5	−39.7 ± 11.9	5.8 ± 0.7
β-hairpin/α_R-β	2 (8.7%)	−57.2 ± 4.2	−47.6 ± 2.7	−74.0 ± 15.0	95.6 ± 0.7	6.5 ± 0.1
α-helix	2 (8.7%)	—	—	—	—	—

[a]Dihedral angles for the middle residues of ideal β-turns are shown in Table I. Dihedral angles (φ_2, ψ_2) correspond to residue Asp6 and (φ_3, ψ_3) correspond to residue Trp7.
[b]This additional criterion for β-turn formation is that the distance of the end residue C_1^α-$C_4^\alpha < 7.0$ Å and the central turn residues are not helical, where C_1^α corresponds to Gln5 and C_4^α corresponds to Gly8. In all individual structures, this criterion was satisfied.

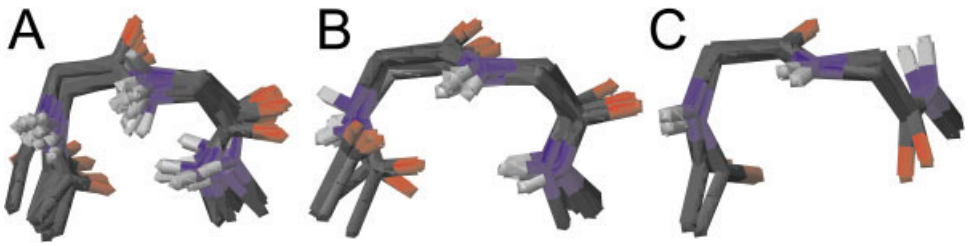

Fig. 5. The β-turn region of the families of MD structures. **A:** Fourteen structures that converged to an α_R-α_R β-turn (coil and β-hairpin). **B:** Five structures that converged to an ε-α_R β-turn. **C:** Two structures that converged to a α_R-β β-turn. The color code is blue for nitrogen, black for carbon, red for oxygen, and gray for hydrogen.

should be noted that there is an agreement between the estimated population of the NMR conformer (42–63% of coil with α_R-α_R β-turn[10]) and the MD conformer with the largest population (43.5% for coil with α_R-α_R β-turn).

Our results provide a measure of the populations of interconverting conformers in compstatin (Figs. 4 and 5). These results also show that even small amplitude backbone motions in the range of 0.1–0.4 Å can result to conformational switch in compstatin (Fig. 6). At longer dynamics (>1 ns), the conformer populations may be altered or more conformers may appear. Here we have demonstrated the flexibility of compstatin and how this flexibility can affect conformational interconversion.

Our results also indicate that the free energy difference between coil and β-hairpin is of the order of 2–5 kcal/mol, between coil and α-helix is of the order of 6 kcal/mol, and between β-hairpin and α-helix is of the order of 3–11 kcal/mol. This finding shows the low free energy barriers involved in conformational interconversion of compstatin. These values correspond to one to six hydrogen bonds,[44] which are responsible for the formation or deformation of secondary structure. When switching from a coil conformation to β-hairpin involving two to three residues per strand, as is compstatin, two to three interstrand hydrogen bonds are formed, depending on the structure model. Compensatory effects may be present because of concurrent switch between β-turn types or change in side-chain hydrogen bond status. Similar arguments hold when switching between coil and α-helix or between β-hairpin and α-helix. Although for small and flexible peptides like compstatin the generalized Born method for solvent representation is typically adequate, an additional MD study using explicit water molecules will be of interest to elucidate the direct effect of water on the stability of individual hydrogen bonds that may affect structure formation.

Overall, during the 1-ns trajectories the residues outside the β-turn segment and inside the cyclic ring can be grouped into residues showing statistical preference for the β-region and residues showing split statistical preference for the β- and α_R-regions of the Ramachandran plot. The former group includes residues Cys2, Val3, Val4, His9, Cys12 (62–92% populations in Fig. 2), and the latter group includes residues His10, Arg11 (47–52% populations in Fig. 2). It is worth noting that from the former group residues, Cys2, Val3, Val4, and Cys12 are part of the hydrophobic cluster of compstatin.[12] From these residues, Cys2 and Cys12 (disulfide bonded) and Val3 are essential to maintain the inhibitory activity of compstatin, whereas Val4 is amenable to further optimization[1,2,10,12] (Klepeis JL, Floudas CA, Morikis D, Tsokos CG, Argyropoulos,E. Spruce L, Lambris JD, Integrated computational and experimental approach for lead optimization and design of compstatin variants with improved activity. Journal of the American Chemical Society 2003: In Press). The remaining residues, His9, His10, Arg11, are part of the polar segment of compstatin, and all of them are amenable to optimization[10,12] (Klepeis JL, Floudas CA, Morikis D, Tsokos CG, Argyropoulos E, Spruce L, Lambris JD, Integrated computational and experimental approach for lead optimization and design of compstatin variants with improved activity. Journal of the American Chemical Society 2003: In Press; Soulika AM, Morikis D, Sarrias

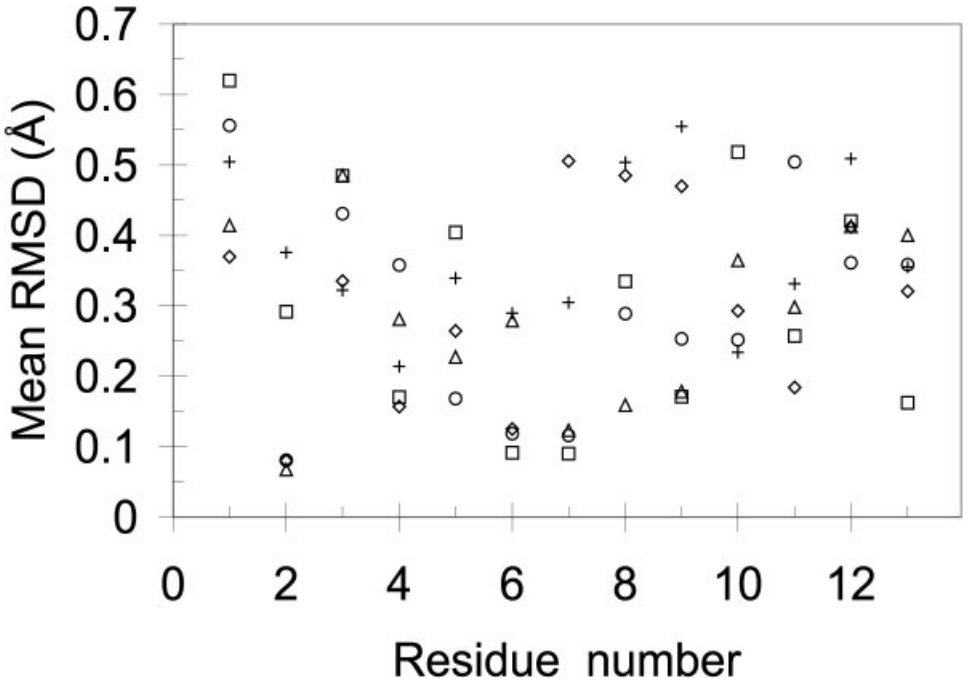

Fig. 6. Plots of mean RMSD between the final MD structures (MD1-21, MDAMS, MDGOS) and initial NMR structures (ES1-21, ESAMS, ESGOS) using backbone heavy atoms for Coil/α_R-α_R family (circles), β-hairpin/α_R-α_R family (squares), β-hairpin/ε-α_R family (triangles), β-hairpin/α_R-β family (diamonds), and α-helix family (crosses).

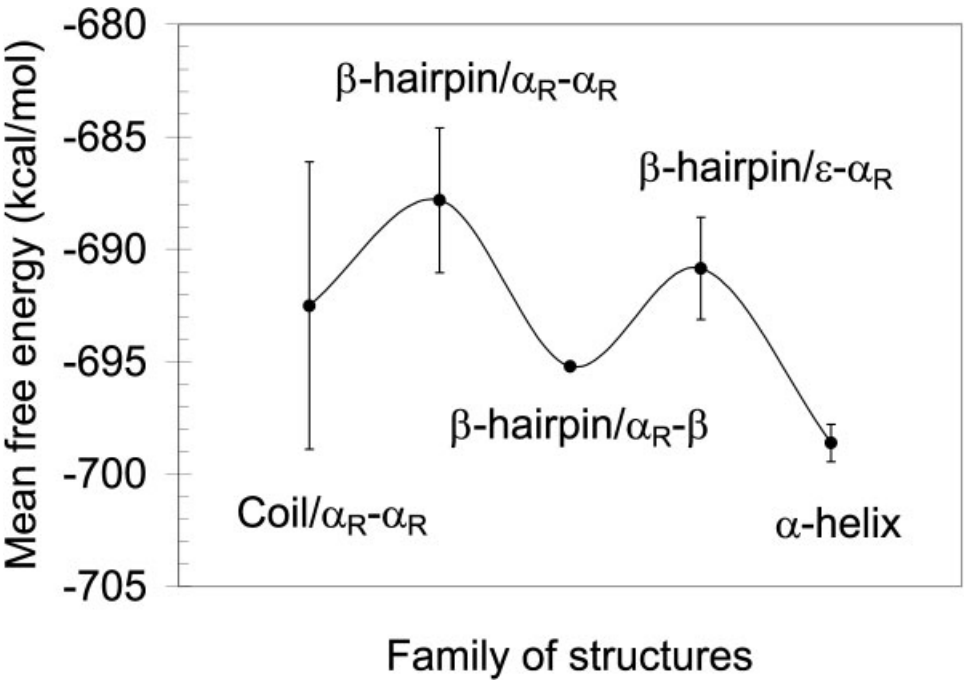

Fig. 7. Plot of the mean free energy minima against the five final MD families of structures. The error bars correspond to standard deviations. This plot indicates the energy barriers for conformational interconversion.

M-R, Roy M, Spruce LA, Sahu A, Lambris JD. Studies of structure-activity relations of complement inhibitor compstatin. Journal of Immunology 2003: In Press). Indeed, SAR-based rational design and rational design-based experimental and computational combinatorial design studies have identified analogs with replacements of Val4 and His9 that are more active than compstatin. These are analogs Ac-H9A, Ac-I1L/H9W/T13G, and Ac-V4Y/H9A[12]

(Soulika AM, Morikis D, Sarrias M-R, Roy M, Spruce LA, Sahu A, Lambris JD. Studies of structure-activity relations of complement inhibitor compstatin. Journal of Immunology 2003: In Press; Klepeis JL, Floudas CA, Morikis D, Tsokos CG, Argyropoulos E, Spruce L, Lambris JD, Integrated computational and experimental approach for lead optimization and design of compstatin variants with improved activity. Journal of the American Chemical Society 2003: In Press). NMR studies for the Ac-H9A and Ac-I1L/H9W/T13G analogs are available and have shown that the β-turn remains intact[12] (Soulika AM, Morikis D, Sarrias M-R, Roy M, Spruce LA, Sahu A, Lambris JD. Studies of structure-activity relations of complement inhibitor compstatin. Journal of Immunology 2003: In Press). It is possible that changes in backbone conformations of residues Val4 and His9 that alter their statistical preference in the (ϕ,ψ) space may be important for modulating the binding ability and inhibitory activity of compstatin.

To date, the most successful optimization of compstatin has been achieved by using a novel computational combinatorial methodology[45,46] that was based on the structural template of compstatin from the NMR data and backbone database-derived potentials (Klepeis JL, Floudas CA, Morikis D, Tsokos CG, Argyropoulos E, Spruce L, Lambris JD, Integrated computational and experimental approach for lead optimization and design of compstatin variants with improved activity. Journal of the American Chemical Society 2003: In Press). This methodology resulted in an 18-fold more active analog than parent peptide compstatin or 7-fold more active analog than acetylated compstatin (Ac-compstatin). Given the conformational interconversion that has been shown by our MD simulations, we are planning to use the additional MD structural templates that correspond to lower populations of alternative but related conformations to pursue further computational combinatorial optimization. The new analog designs will be then tested for activity to establish dynamics-activity relations (DAR).

CONCLUSIONS

In summary, we have demonstrated the presence of five interconverting conformers in compstatin using the original NMR structures and MD simulations. At 1 ns, each of these conformers has populations between ~9 and 44%. From the initial 21 individual structures of the ensemble, 10 converged to similar conformations after the 1-ns MD simulations (coiled/α_R-α_R) and 14 converged an α_R-α_R β-turn. The structures of the five conformers can be used as structural templates for further optimization in the design of compstatin, which can result in higher inhibitory activity. We believe that it is necessary to incorporate the presence of more than one conformer into our thinking, within our rational or combinatorial optimization, for compstatin and for peptide-drug design in general. NMR data of ensembles of structures may be more suitable for MD simulations of peptides, rather than single crystallographic structures.

ACKNOWLEDGMENTS

This work was supported by the American Heart Association, Western States Affiliate (DM) and the National Institutes of Health (JDL, DM). We thank Dr. Richard Henchman for critical reading of the manuscript and for helpful suggestions.

REFERENCES

1. Sahu A, Kay BK, Lambris JD. Inhibition of human complement by a C3-binding peptide isolated from a phage-displayed random peptide library. J Immunol 1996;157:884–891.
2. Sahu A, Soulika AM, Morikis D, Spruce L, Moore WT, Lambris JD. Binding kinetics, structure-activity relationship, and biotransformation of the complement inhibitor compstatin. J Immunol 2000; 165:2491–2499.
3. Furlong ST, Dutta AS, Coath MM, Gormley JJ, Hubbs SJ, Lloyd D, Mauger RC, Strimpler AM, Sylvester MA, Scott CW, Edwards PD. C3 activation is inhibited by analogs of compstatin but not by serine protease inhibitors or peptidyl alpha-ketoheterocycles. Immunopharmacology 2000;48:199–212.
4. Sahu A, Morikis D, Lambris JD. Complement inhibitors targeting C3, C4, and C5. In: Lambris JD, Holers VM, editors. Therapeutic interventions in the complement system. Totowa, NJ: Humana Press, 2000;9:75–112.
5. Sahu A, Lambris JD. Complement inhibitors: a resurgent concept in anti-inflammatory therapeutics. Immunopharmacology 2000;49: 133–148.
6. Soulika AM, Khan MM, Hattori T, Bowen FW, Richardson BA, Hack CE, Sahu A, Edmunds LH Jr, Lambris JD. Inhibition of heparin/protamine complex-induced complement activation by Compstatin in baboons. Clin Immunol 2000;96:212–221.
7. Fiane AE, Mollnes TE, Videm V, Hovig T, Hogasen K, Mellbye OJ, Spruce L, Moore WT, Sahu A, Lambris JD. Compstatin, a peptide inhibitor of C3, prolongs survival of ex vivo perfused pig xenografts. Xenotransplantation 1999;6:52–65.
8. Fiane AE, Mollnes TE, Videm V, Hovig T, Hogasen K, Mellbye OJ, Spruce L, Moore WT, Sahu A, Lambris JD. Prolongation of ex vivo-perfused pig xenograft survival by the complement inhibitor Compstatin. Transplant Proc 1999;31:934–935.
9. Nilsson B, Larsson R, Hong J, Elgue G, Ekdahl KN, Sahu A, Lambris JD. Compstatin inhibits complement and cellular activation in whole blood in two models of extracorporeal circulation. Blood 1998;92:1661–1667.
10. Morikis D, Assa-Munt N, Sahu A, Lambris JD. Solution structure of Compstatin, a potent complement inhibitor. Protein Sci 1998;7: 619–627.
11. Klepeis JL, Floudas CA, Morikis D, Lambris JD. Predicting peptide structures using NMR data and deterministic global optimization. J Comp Chem. 1999;20:1354–1370.
12. Morikis D, Roy M, Sahu A, Troganis A, Jennings PA, Tsokos GC, Lambris JD. The structural basis of compstatin activity examined by structure- function-based design of peptide analogs and NMR. J Biol Chem 2002;277:14942–14953.
13. Brooks BR, Bruccoleri RE, Olafson BD, States DJ, Swaminathan S, Karplus M. CHARMM: a program for macromolecular energy, minimization and dynamics calculations. J Comp Chem 1983;4: 187–217.
14. Still WC, Tempczyk A, Hawley RC, Hendrickson T. Semianalytical treatment of solvation for molecular mechanics and dynamics. J Am Chem Soc 1990;112:6127–6129.
15. Dominy B, Brooks CLI. Development of a generalized Born model parameterization for proteins and nucleic acids. J Phys Chem 1999;103:3765–3773.
16. Ryckaert J-P, Cicotti G, Berendsen HC. Numerical integration of the Cartesian equations of motion of a system with constraints: molecular dynamics of n-alkanes. J Comput Phys 1977;23:327–341.
17. Wilmot CM, Thornton JM. Beta-turns and their distortions: a proposed new nomenclature. Protein Eng 1990;3:479–493.
18. Kabsch W, Sander C. Dictionary of protein secondary structure: pattern recognition of hydrogen-bonded and geometrical features. Biopolymers 1983;22:2577–2637.
19. Koradi R, Billeter M, Wuthrich K. MOLMOL: a program for

display and analysis of macromolecular structures. J Mol Graph 1996;14:51–55, 29–32.
20. Wilmot CM, Thornton JM. Analysis and prediction of the different types of β-turns in proteins. J Mol Biol 1988;203:221–232.
21. Thornton JM, Sibanda BL, Edwards MS, Barlow DJ. Analysis, design and modification of loop regions in proteins. Bioessays 1988;8:63–69.
22. Hutchinson EG, Thornton JM. A revised set of potentials for beta-turn formation in proteins. Protein Sci 1994;3:2207–2216.
23. Venkatachalam CM. Stereochemical criteria for polypeptides and proteins. V. Conformation of a system of three linked peptide units. Biopolymers 1968;6:1425–1436.
24. Lewis PN, Momany FA, Scheraga HA. Chain reversals in proteins. Biochim Biophys Acta 1973;303:211–229.
25. Chou PY, Fasman GD. Beta-turns in proteins. J Mol Biol 1977;115: 135–175.
26. Richardson JS. The anatomy and taxonomy of protein structure. Adv Protein Chem 1981;34:167–339.
27. Rose GD, Gierasch LM, Smith JA. Turns in peptides and proteins. Adv Protein Chem 1985;37:1–109.
28. Chou KC. Prediction of tight turns and their types in proteins. Anal Biochem 2000;286:1–16.
29. Dyson HJ, Wright PE. Defining solution conformations of small linear peptides. Annu Rev Biophys Biophys Chem 1991;20:519–538.
30. Dyson HJ, Wright PE. Antigenic peptides. FASEB J 1995;9:37–42.
31. Dyson HJ, Cross KJ, Houghten RA, Wilson IA, Wright PE, Lerner RA. The immunodominant site of a synthetic immunogen has a conformational preference in water for a type-II reverse turn. Nature 1985;318:480–483.
32. Dyson HJ, Rance M, Houghten RA, Lerner RA, Wright PE. Folding of immunogenic peptide fragments of proteins in water solution. I. Sequence requirements for the formation of a reverse turn. J Mol Biol 1988;201:161–200.
33. Dyson HJ, Rance M, Houghten RA, Wright PE, Lerner RA. Folding of immunogenic peptide fragments of proteins in water solution. II. The nascent helix. J Mol Biol 1988;201:201–217.
34. Osterhout JJ Jr, Baldwin RL, York EJ, Stewart JM, Dyson HJ, Wright PE. 1H NMR studies of the solution conformations of an analogue of the C- peptide of ribonuclease A. Biochemistry 1989;28: 7059–7064.
35. Merutka G, Morikis D, Bruschweiler R, Wright PE. NMR evidence for multiple conformations in a highly helical model peptide. Biochemistry 1993;32:13089–13097.
36. Bruschweiler R, Morikis D, Wright PE. Hydration of the partially folded peptide RN-24 studied by multidimensional NMR. J Biomol NMR 1995;5:353–356.
37. Millhauser GL, Stenland CJ, Hanson P, Bolin KA, van de Ven FJ. Estimating the relative populations of 3_{10}-helix and alpha-helix in Ala-rich peptides: a hydrogen exchange and high field NMR study. J Mol Biol 1997;267:963–974.
38. Blanco FJ, Jimenez MA, Herranz J, Rico M, Santoro J, Nieto JL. NMR evidence of a short linear peptide that folds into a β-hairpin in aqueous solution. J Am Chem Soc 1993;115:5887–5888.
39. Ramirez-Alvarado M, Blanco FJ, Serrano L. De novo design and structural analysis of a model beta-hairpin peptide system. Nat Struct Biol 1996;3:604–612.
40. Santiveri CM, Santoro J, Rico M, Jimenez MA. Thermodynamic analysis of beta-hairpin-forming peptides from the thermal dependence of ^{1}H NMR chemical shifts. J Am Chem Soc 2002;124:14903–14909.
41. Sharman GJ, Searle MS. Cooperative interaction between the three strands of a designed antiparallel beta-sheet. J Am Chem Soc 1998;120:5291–5300.
42. Das C, Raghotharna S, Balaram P. A designed three stranded beta-sheet peptide as a multiple beta-hairpin model. J Am Chem Soc 1998;120:5812–5813.
43. Gibbs AC, Bjorndahl TC, Hodges RS, Wishart DS. Probing the structural determinants of type II′ beta-turn formation in peptides and proteins. J Am Chem Soc 2002;124:1203–1213.
44. Brooks CLI. Protein and peptide folding explored with molecular simulations. Acc Chem Res 2002;35:447–454.
45. Klepeis JL, Floudas CA. Free energy calculations for peptides via deterministic global optimization. J Chem Phys 1999;110:7491–7512.
46. Klepeis JL, Floudas CA. Ab initio tertiary structure prediction of proteins. J Glob Optimiz 2003;25:113–140.